Nanoindentation and nanoscratching of rutile and anatase TiO_2 studied using molecular dynamics simulations

2008 J. Phys.: Condens. Matter 20 354010

(http://iopscience.iop.org/0953-8984/20/35/354010)

IOP PUBLISHING JOURNAL OF PHYSICS: CONDENSED MATTER

J. Phys.: Condens. Matter **20** (2008) 354010 (10pp) doi:10.1088/0953-8984/20/35/354010

Nanoindentation and nanoscratching of rutile and anatase TiO_2 studied using molecular dynamics simulations

I Gheewala, R Smith and S D Kenny

Department of Mathematical Sciences, Loughborough University, Loughborough LE11 3TU, UK

Received 1 February 2008, in final form 12 March 2008
Published 11 August 2008
Online at stacks.iop.org/JPhysCM/20/354010

Abstract

The results of molecular dynamics (MD) simulations of nanoindentation and nanoscratching of titanium dioxide lattices are presented. The TiO_2 surfaces investigated are the (001) and {110} rutile surfaces and the anatase {100} and (001) surfaces. A spring model consisting of a cube cornered indenter connected to supports, via a set of springs, was used to model the cantilever in an atomic force microscope. Indentations were conducted to depths of 12 and 18 Å on each surface and scratching simulations were conducted for a length of 80 Å and at a depth of 6 Å. Pile-up patterns were found to be dependent on the crystal surface orientation. No evidence of the activation of slip systems was discovered. The relative values of the contact pressure and Young's modulus were in reasonable agreement with experiment and the coefficient of friction was found to be independent of the TiO_2 polymorph.

(Some figures in this article are in colour only in the electronic version)

1. Introduction

With the increased use of materials on the nanometre scale it has become more important to understand the behaviour of materials on such a scale. Since a material's mechanical properties, such as the hardness and Young's modulus may vary depending on the scale, they need to be determined specifically for the nanoscale. An indentation into a sample of material using a hard tip is one method for finding how it will behave under stress. For materials that are to be used on the nanoscale in applications such as a thin films, investigating the properties is difficult using traditional indentation experiments. Information obtained from such an experiment would be significantly influenced by the substrate, unless the penetration depth is much smaller than the coating thickness.

The nanoindentation technique has been developed to provide a method of indenting into a material on the nanoscale. Tools such as the atomic force microscope (AFM) allow indentations and scratches to be made at depths as small as 10 nm. Recently, computer simulations using molecular dynamics (MD) have allowed the simulation of nanoindentation and nanoscratching [1–9]. Such a simulation is able to complement data from an experiment by monitoring the behaviour of specific atoms as well as that of the material beneath the surface. Indentation simulations are generally conducted on a smaller scale than experiment but if they have a good model of the interatomic forces, they can accurately reproduce pile-up patterns and force–depth curves.

In this work MD simulations were carried out on different surfaces of the rutile and anatase polymorphs of titanium dioxide. The motivation for investigating the TiO_2 rutile and anatase polymorphs is due to their use in optical coatings. Both rutile and anatase have very good optical properties, with rutile used in anti-reflective coatings and anatase for its excellent hydrophilicity [10, 11]. The form of TiO_2 used in thin films has a high dependence on the method of deposition as well as the temperature and pressure under which annealing takes place. Therefore, the layers of TiO_2 can be grown according to which property is of greater importance for the particular application being considered.

Rutile has a tetragonal unit cell and is found in the cassiterite form belonging to the D_{4h}^{14} ($P4/mnm$) space group (figure 1). The tetragonal unit cell of anatase is more elongated than rutile and belongs to the D_{4h}^{19} ($I4/amd$) space group (figure 2). In both polymorphs titanium atoms are surrounded by six oxygen atoms and each oxygen atom is three fold coordinated [12]. Rutile, the most common and naturally occurring form of TiO_2 had indentation and

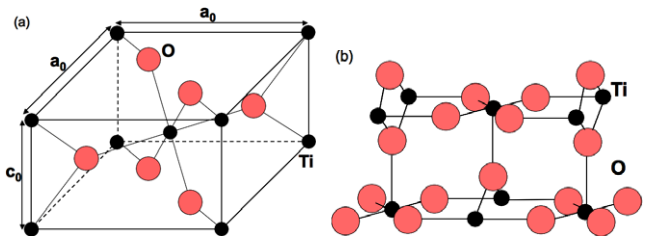

Figure 1. The unit cell of the rutile form of TiO_2 (a) and the {110} (1 × 1) reconstructed surface (b). The titanium and oxygen atoms are represented by the small and large spheres respectively. The lattice parameters from Wyckoff [12] are $a_0 = 4.594$ Å and $c_0 = 2.958$ Å.

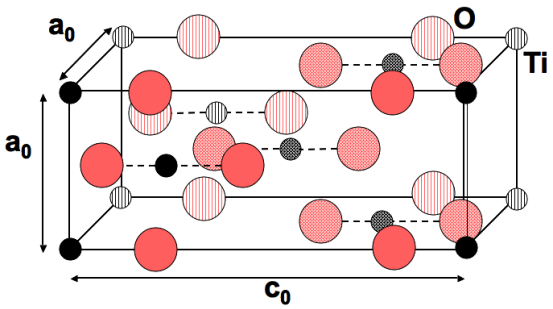

Figure 2. The unit cell of the anatase form of TiO_2 with the {100} surface on top. Atoms are shaded according to depth with solid atoms at the front, shaded atoms half way back, and striped atoms at the far end of the cell, The small spheres are titanium atoms with the larger spheres showing oxygen atoms. The lattice parameters from Wyckoff [12] are $a_0 = 3.785$ and $c_0 = 9.514$.

scratching simulations performed on the stoichiometric (001) surface and the experimentally stable {110} surface. Many different proposals have been put forward for the exact reconstruction of the rutile {110} surface, however, the stoichiometric (1 × 1) reconstruction [13] was used since it was the most stable surface under room temperature and pressure. The anatase polymorph of TiO_2 which occurs as a thin film had indentations and scratches conducted on the {100} and (001) surfaces. The anatase (001) surface used for simulations was the stoichiometric (1 × 1) surface, however, a (4 × 1) reconstruction has also been proposed [14]. The anatase (001) surface was chosen due to being the favourable surface and is often used to grow other films [15].

2. Methodology

The model used for the simulations conducted in this work is known as the spring model and is based on the AFM cantilever indenter [4–6]. Figure 3 shows a representation of the indenter and substrate setup used. The stiffness of the springs were kept constant for all simulations and had a value comparable to the stiffness of the AFM cantilever. The initial stage of each simulation was the same, support B pushing the indenter into the material in the y-direction with a constant velocity of 10 m s^{-1} until the apex of the indenter reached a specified depth. For each surface indents were conducted to a depth of 12 and 18 Å after which support B was held still for a period of

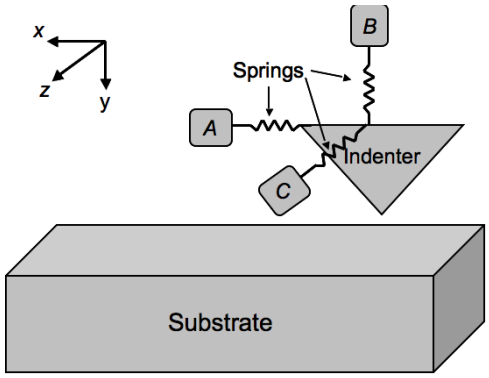

Figure 3. The MD model used for simulations is setup with the indenter connected to a series of supports via a set of springs, with each support controlling the indenter motion in each direction. Support B is pushed down during the indentation stage, and scratching is conducted in the x-direction by pulling support A.

10 ps to allow the system to relax before the retraction of the tip at the same constant speed of 10 m s^{-1} with the simulation ending once the indenter was far enough from the material so that there was no interaction between the two. For the nanoscratching simulation, once the indenter apex reached a depth of 6 Å there was again a holding period of 10 ps, and then support A was used to pull the indenter in the x-direction along the surface of the material at a velocity of 10 m s^{-1}. Each surface was scratched for a distance of about 80 Å.

Each indentation simulation was performed using a substrate lattice of size 13 nm × 9 nm × 13 nm, with the shorter distance indicating the depth of the lattice. This gave between about 140 000 atoms for the less dense anatase, and about 166 000 atoms in the rutile lattices. Scratch simulations were conducted on lattices of size 16 nm × 6 nm × 10 nm, with the longest dimension indicating the scratch direction. Atom numbers in these lattices varied between about 83 000 and 93 000 depending on the density of the polymorph.

The indenter chosen for the simulations was the diamond cube cornered indenter which is formed at the apex of 3 intersecting {100} faces of a diamond cube, giving a 90° triangular-based pyramidal indenter with the {111} surface as the base. The interaction between the atoms of the indenter were modelled using the many-body Brenner potential energy function [16, 17]. The interaction between the tip and the lattice was modelled as purely repulsive, therefore the short ranged, Ziegler–Biersack–Littmark (ZBL) potential [18] was used.

Interactions between atoms within the titania polymorphs were modelled using the pair potential parameterized by Matsui and Akaogi [19], which describes the energy from the interaction of atoms i and j as

$$V_{ij} = \frac{q_i q_j}{r_{ij}} - \frac{C_i C_j}{r_{ij}^6} + f(B_i + B_j)\mathrm{e}^{\frac{A_i + A_j - r_{ij}}{B_i + B_j}} \qquad (1)$$

where the terms represent the Coulomb, dipole and repulsion interactions respectively. Atoms i and j are separated by a distance of r_{ij}, and q_i, A_i, B_i and C_i are the effective charge, repulsive radius, softness parameter, and van der

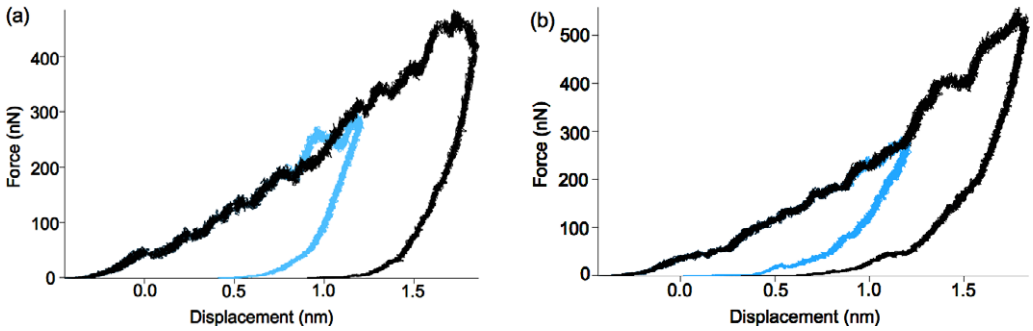

Figure 4. The force depth curves obtained from indenting into the (001) surface (a) and the {110} (1 × 1) reconstructed surface (b) of rutile. The lighter curves show indents conducted to a depth of 12 Å, the dark curves show indents to a depth of 18 Å.

Waals coefficient respectively and are given by Matsui and Akaogi [19].

The lattice parameters for rutile obtained by Matsui and Akaogi were utilized for the simulations as these are very close to those found experimentally [12]. The Coulombic term is a long ranged term and is computationally very expensive, to evaluate it a fast multipole method was used to provide an approximation to this energy contribution [20].

When setting up the systems the first 3 layers of atoms in each non indenting surface of the lattice were held fixed as well as the top two layers of indenter atoms to which the springs were connected. All other atoms in the system were relaxed to obtain a minimum energy state. Once fully relaxed the systems were heated to a temperature of 300 K using a Berendsen thermostat [21]. Initially all free atoms within the lattice and indenter were heated to the required temperature, after which the first 5 free atomic layers in the non indenting surfaces were set as thermostat atoms. These atoms maintained the temperature by dissipating excess heat during the simulation stages. During the relaxing and heating stages, the indenter was kept well away from the surface of the lattice so that no interactions occurred. Once the system was stabilized at 300 K the indenter was moved closer to the lattice so that the distance of the apex from the surface was just outside the cutoff radius used for the ZBL potential.

Once setup, the subsequent motion of the atoms was described by the gradient of the potential energy functions which yields the force on each atom. Newton's equation of motion could then be solved, with the new positions and velocities of each atom given by a numerical integration algorithm. The velocity Verlet algorithm was chosen since it has been shown to have good energy conservation properties as well as being computationally efficient [22, 23]. A fixed time step of 1 fs was implemented for all simulations, which has been found to be suitable for accurately modelling ionic materials.

The main difference with experiments is that these are performed generally with a fixed force at slower loading rates, and at much greater depths than currently accessible through simulations. Because of system size constraints, the indentation simulations take place to a fixed maximum depth, and, because of computing time requirements, at faster loading rates.

3. Results

3.1. Nanoindentation

As with experimental nanoindentions, the force acting on the indenter was plotted against the depth of the apex into the surface. Figure 4 shows the force depth curves obtained from indentations into the (001) and {110} surfaces of rutile. The small steps seen on the loading sections of the force depth curves are known as pop-in events and describe sudden movements of the indenter into the material to relieve the force once it builds up to a critical level. Often a pop-in event coincides with the activation of a slip system, however, no such slip systems were seen to be activated in either of the orientations. The pop-in events are quite small and not very distinct and similarly the damage in the crystal occurring at these points is relatively small, corresponding to a local transformation from crystalline to amorphous. Even the most significant pop-in event in the deeper rutile {110} indent, when a force of about 400 nN is applied, does not correspond to the activation of any significant slip system.

There is a considerable difference in the forces applied to the indenter during the indentation process for the two rutile surfaces. The indentation into the (001) surface has a peak force of 480 nN during the 18 Å indent, which is much smaller than the 550 nN applied when the indenter reaches the peak depth during the indentation into the {110} surface, suggesting that the {110} surface is much harder.

During the retraction stage of the simulations some elastic recovery of the material can be seen as the indenter withdraws from the surface. A significant difference is also seen in the residual depth of the two rutile surfaces. This is the point at which the indenter loses contact with the surface and occurs when the force depth curve reaches zero. Looking at the deeper indents in the rutile (001) surface, the apex loses contact when at a depth of about 11 Å, however, there appears to be much more elastic recovery in the rutile {110} surface where contact remains until the apex is only about 7 Å into the surface.

During the indentation process material displaced by the indenter forms pile-up around the indentation site. The magnitude and arrangement of the pile-up varies depending on the material and the mechanisms which cause the displacement. Often pile-up will be created by the activation of slip systems and the action of cross slip which brings material

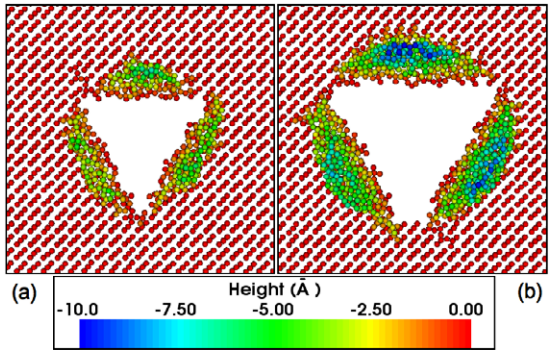

Figure 5. The surface pile-up created after indentions into the rutile (001) surface to depths of 12 Å (a) and 18 Å (b).

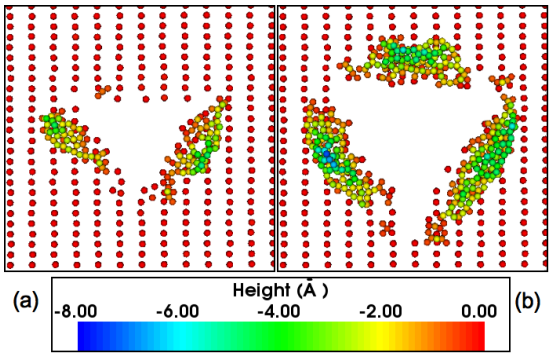

Figure 6. The surface pile-up created after indenting into the rutile {110} (1 × 1) reconstructed surface to a depth of 12 Å (a) and 18 Å (b).

to the surface. Figures 5 and 6 show that the pile-up created during indentation into the rutile (001) and {110} surfaces differs considerably. The pile-up of material in figure 5 shows a symmetric formation of pile-up around the indentation site. The deeper indent has caused pile-up which peaks at ∼10 Å.

In comparison, there is much less pile-up created on the rutile {110} surface as shown in figure 6, with a maximum height of almost 8 Å in the 18 Å indent. The packing of the material on the {110} surface is much less dense than on the (001) surface. The deeper indent has pile-up formed almost symmetrically around the three sides of the imprint, whereas, the shallower 12 Å indent has one side of the indent creating virtually no pile-up. The other two sides of the smaller indent do have some pile-up, but again it is far less than that seen in the (001) surface for the same indentation depth, and consists of only two atomic layers of adatoms.

Often an indentation into a material will cause the activation of a number of slip systems due to the stresses applied. However, the indentation simulations into both the rutile (001) and {110} (1 × 1) reconstructed surface failed to activate any distinct slip systems. Figure 7 plots the slip vector and shows that there are no visible patterns in the atoms that have slipped beneath the indented region. Despite the lack of slip in the simulations, it has been found experimentally that there are a number of slip systems in rutile TiO_2 [24–26]. Slip along the {101} plane in the $\langle\bar{1}01\rangle$ is said to be activated at a temperature of 875 K, and at 1175 K slip is thought to occur in

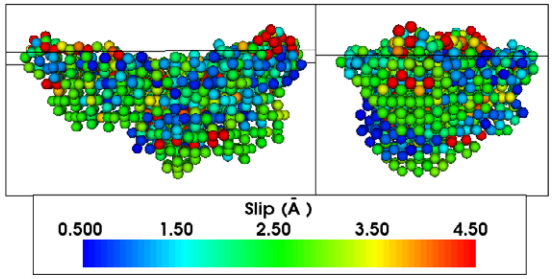

Figure 7. The slip activated shortly after the indenter reached peak depth during the 18 Å indentation simulation into the rutile {110} surface.

{110} plane in a ⟨001⟩ direction. The magnitude of the Burgers vector in the former slip plane is $\frac{1}{2}\langle\bar{1}01\rangle$ (2.71 Å) with the slip occurring on the titanium sub lattice and the oxygen atoms remaining relatively undisturbed. The second slip system has a Burgers vector ⟨100⟩ of magnitude 3.02 Å. Figure 7 covered atoms that had slipped over a large range of possible values. Figure 8 shows atoms that have slipped in the same simulation, but with ranges matching the Burgers vectors of the above slip systems. Having filtered out the other atoms, one can see that there is no evidence of concerted slip motion.

Figure 9 gives a diagrammatic representation of atoms in the anatase {100} surface. Distinct rows can be thought of as having been formed by atoms on opposing elongated faces of the crystal cell structure shown in figure 2. Figure 9 shows that when setting up the indentation simulations into the {100} surface, the indenter can be positioned so that one side of the indenter is either perpendicular (orientation A) or parallel (orientation B) to these rows.

The indentations into the anatase {100} surface at depths of 12 and 18 Å with the indenter in orientations A and B produced the force depth curves shown in figure 10. The forces in action when indenting into the anatase surfaces are far less than those for the rutile indentations in figure 4, with a maximum force of just over 300 and 270 nN for orientation A and B respectively which compares to about 480 and 550 nN for indentations into the rutile (001) and {110} surfaces. The smaller forces required to indent anatase to a similar depth to rutile is due to the less dense structure of anatase. There is a small difference in forces when indenting using orientation A and B in the anatase {100} surfaces, with orientation A requiring a larger force to reach the same indentation depth.

As with the indentations into rutile, there are pop-in events during indentations into anatase {100} surfaces, however, they are again small in nature and do not activate any particular slip systems and only small displacements of atoms occur. The retraction phase of the simulations into anatase {100} are almost identical for both indenter orientations at the same depth of indent. The recovery of the material is such that the indenter and substrate contact is maintained until the indenter apex reaches a depth of about 10 Å in the deeper 18 Å indents and just over 5 Å in the shallower 12 Å indents. When comparing the anatase {100} recovery to that in the rutile systems, there is slightly less recovery in the rutile (001) indents, but far more recovery in the rutile {110}.

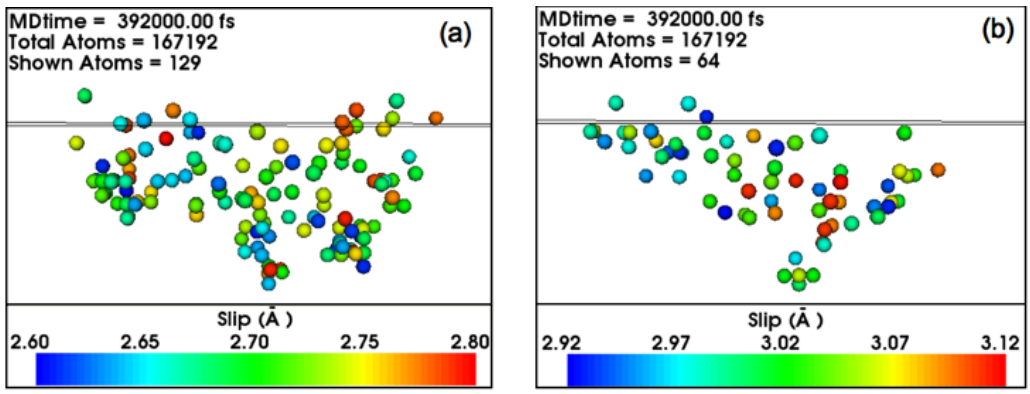

Figure 8. The slip during the 18 Å indentation simulation into the rutile {110} (1 × 1) reconstructed surface. The images show atoms that have slipped with a Burger's vector close to 2.71 Å (a), and 3.02 Å (b). These values correspond to the {101} ⟨$\bar{1}$01⟩ and {110} ⟨001⟩ slip systems, respectively.

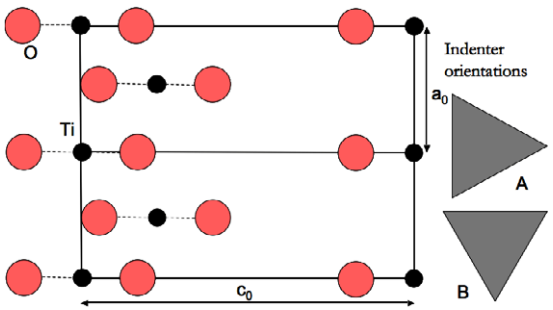

Figure 9. A diagrammatic representation of the anatase {100} surface with distinct atomic rows that run parallel to the crystal axis. The two tip orientations A and B have been used for indenting.

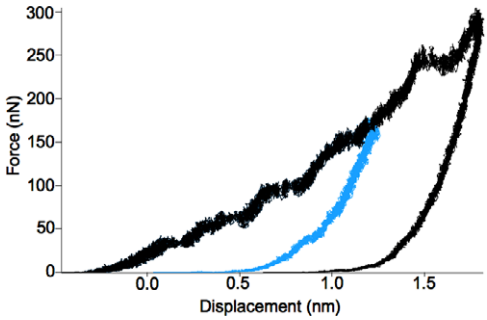

Figure 11. The force depth curve from the indentation simulation into the (001) anatase surface. The lighter curve shows the 12 Å indentation and the dark curve shows the indentation to 18 Å.

The anatase (001) surface was also indented to depths of 12 and 18 Å, with the force depth curves shown in figure 11. The force depth curve has very similar characteristics to those obtained from indentations into the {100} surface in orientation A.

The pile-up of atoms in the anatase {100} indentations shown in figures 12 and 13 is far less than that seen in the rutile simulations. The maximum is only 2 atomic layers in height after the 18 Å indents. These figures also show that there is residual strain in the lattice after the extraction of the indenter which is most marked in orientation A in figure 12, with a 'bowing out' of the atomic rows parallel to an edge of the indenter. Along the direction where the indenter edge is parallel to the crystalline axis there is also less pile-up. When the crystal is rotated through 90° (figure 13) the effect is less marked, and the pile-up is more evenly distributed.

The pile-up created on the surface of the anatase (001) lattices after the indentations to 12 and 18 Å can be seen in figure 14. Although the maximum height of the pile-up is again 2 atomic layers in height, the magnitude of the pile-up is far greater. Although clearer in the 18 Å indent, at both depths the pile-up is asymmetric, with less pile-up seen on the edge where

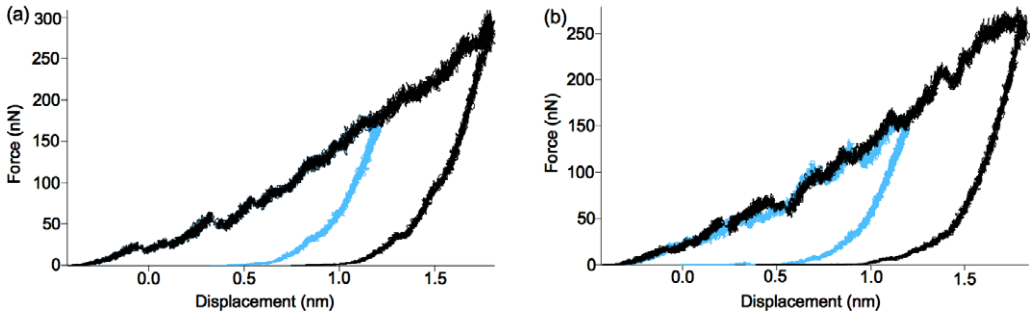

Figure 10. The force depth curves obtained from indenting into the {100} anatase surfaces with the indenter orientation A (a) and B (b). The light curves show indentations conducted to a depth of 12 Å, the dark curves are the 18 Å indentations.

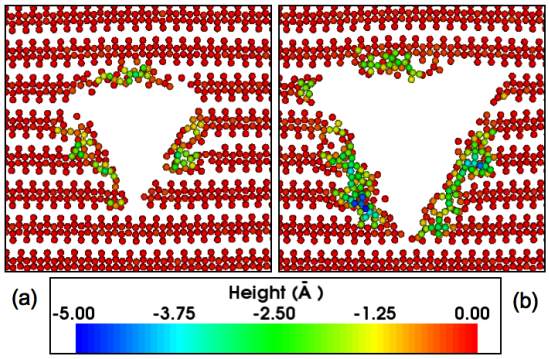

Figure 12. The surface pile-up after indenting into the anatase {100} surface with indenter orientation A. Image (a) is after indenting to 12 Å and image (b) after an 18 Å indent.

Table 1. Contact pressures calculated from the indentations into the TiO_2 surfaces. The experimental values [11] relate to thin films, however, specific details are not available, so values are used only as a guide.

Surface	Contact pressure (GPa)	Experimental contact pressure (GPa)
Rutile (001)	27.3	17
Rutile {110}	30.8	
Anatase {100}	17.8	8
Anatase (001)	19.0	

the side of the indenter runs parallel to the ⟨100⟩ direction. The total number of atoms piled up on the anatase (001) surface is similar to the rutile {110} surface, but spread out more, with a slightly lower peak height. Some residual strain is seen in the indentations at this orientation, as seen in the anatase {100} surface. This is especially clear in the 12 Å indent shown in figure 14. The 'bowing out' of the surface is illustrated by the chains of atoms starting from the indenter sides marked by the arrow A in the diagram.

The contact pressure (hardness) is one of the key mechanical properties obtained from conducting a nanoindentation into a material and is defined by

$$\frac{F_{\max}}{A}, \tag{2}$$

where $F_{\max}$ is the normal force exerted on the indenter at the maximum depth at which point the cross sectional contact area is A. In a nanoindentation experiment A is usually determined using the Oliver and Pharr method [27]. With a nanoindentation simulation this contact area is directly measurable from the computer visualization of the system.

Table 1 shows the contact pressure values obtained from the various TiO_2 surfaces. The values for the contact pressure for rutile and anatase systems are in the correct ratio relative to experiment. The fixed boundaries of the lattice are known to create an artificial hardness in the simulations [28], and for other materials this can cause the contact pressure to be overestimated by a factor of 2. It is also known that many materials experience an indentation size effect at small indentation depths. Thus the calculated values of hardness

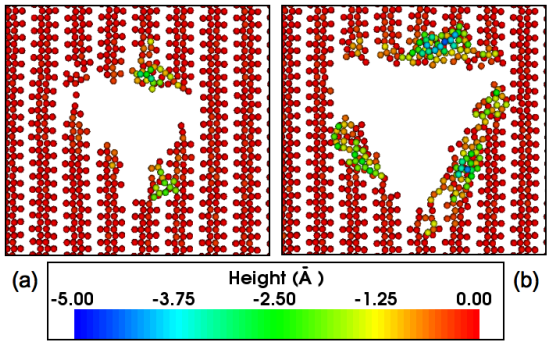

Figure 13. The surface pile-up after indentations into the anatase {100} surface with the indenter in orientation B. Image (a) is after indenting to 12 Å and the image (b) after an 18 Å indent.

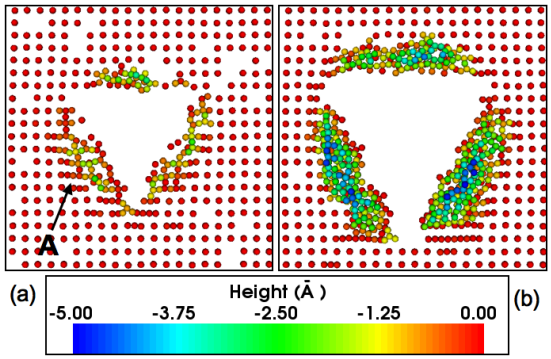

Figure 14. The surface pile-up after the 12 Å (a) and 18 Å (b) indentation simulations into the anatase (001) surface.

should be seen more in a relative context than taken as absolute numbers.

The Young's modulus, E, of a material is an important mechanical property and is a measure of a materials stiffness that can be determined from a nanoindentation experiment [27, 29]. The reduced Young's modulus, E_r, of a material can be calculated using

$$\frac{1}{E_r} = \frac{(1-v^2)}{E} + \frac{(1-v_i^2)}{E_i}, \tag{3}$$

where v and v_i are the Poisson's ratio of the substrate and indenter, and E and E_i are the Young's modulus of the surface and indenter respectively. Using the stiffness, S, from the initial portion of the unloading curve, the reduced Young's modulus can be calculated with the usual Oliver and Pharr formula

$$S = \frac{dP}{dh} = \frac{2}{\sqrt{\pi}} E_r \sqrt{A}. \tag{4}$$

The dP/dh is the tangent to the initial unloading curve, h is the depth and A is the contact area.

The Young's modulus values obtained from the nanoindentations into the rutile and anatase TiO_2 surfaces, shown in table 2, vary depending on the surface indented. Overall, the Young's modulus values are in reasonable agreement with the experimental values. The discrepancies in the results may be due to a number of different factors in addition to the fixed

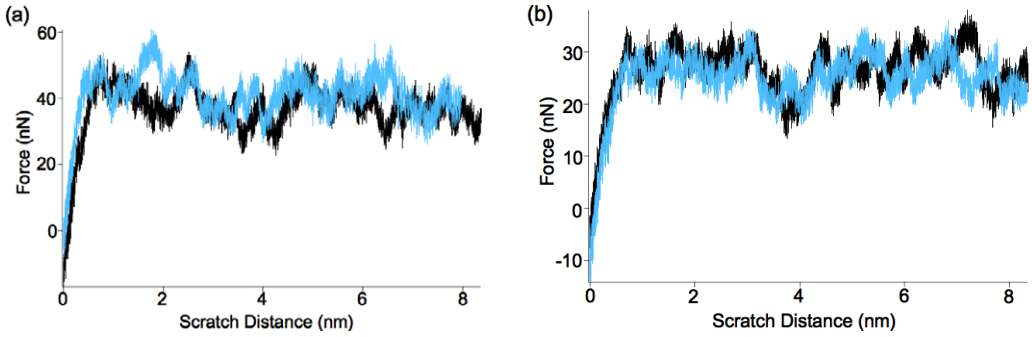

Figure 15. The lateral forces during the scratches into the rutile (a) (001) (light) and {110} (1 × 1) reconstructed (dark) surfaces and the anatase (b) {100} (dark) and (001) (light) surfaces.

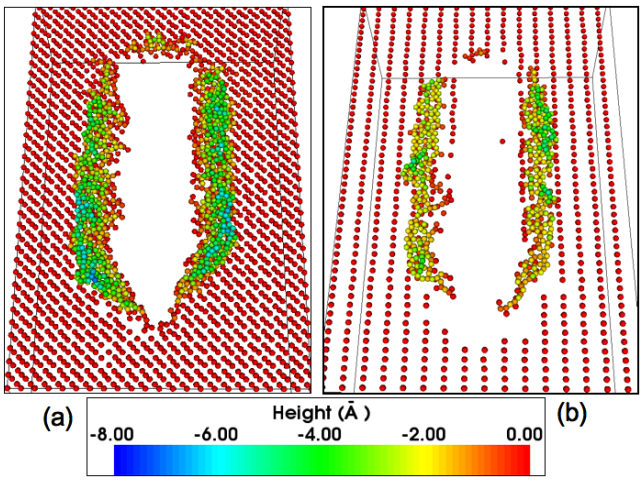

Figure 16. The pile-up of material during the 6 Å deep scratches into the rutile (001) (a) and {110} (1 × 1) reconstructed (b) surfaces.

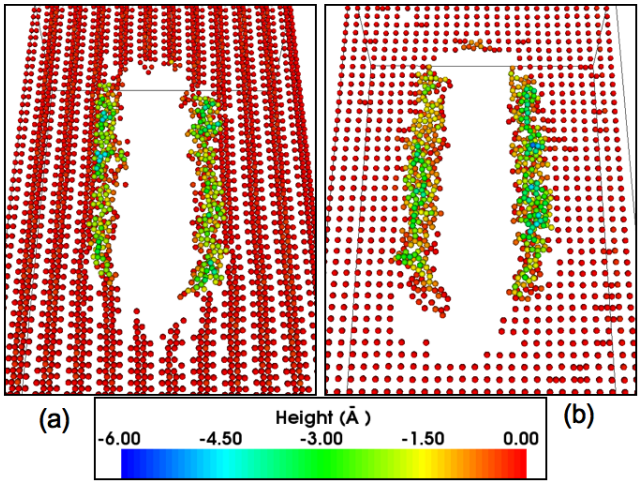

Figure 17. The pile-up of material during the 6 Å deep scratches into the anatase {100} (a) and {001} (b) surfaces.

Table 2. The Young's modulus calculated from the indentation simulations into the rutile and anatase TiO_2 surfaces compared to experimental values [11].

Surface	Young's modulus(GPa)	Experimental Young's modulus (GPa)
Rutile (001)	379	260
Rutile {110}	316	
Anatase {100}	192	170
Anatase (001)	170	

boundary conditions, such as the difficulty in measuring the slope accurately, an inadequate holding time, the smaller scale of the simulation compared to experiment and the faster indentation speeds used.

3.2. Nanoscratching

During the nanoscratching simulations, forces applied to the indenter in the directions shown in figure 3 are recorded. Of interest is the force in the scratch direction during the simulation which is logged and plotted against the scratch distance and shown in figure 15 for the rutile and anatase surfaces. The scratch along the anatase {100} surface was set up such that indenter orientation B was used, giving an indenter to surface relationship as shown in figure 9. The forces applied to the indenter in the scratching direction during the two rutile simulations, as with the indentations, was considerably greater than the forces required to scratch the two anatase surfaces. While the forces differ between the rutile and anatase, the surface being scratched for each polymorph does not seem to affect the force. The first 10 Å of the scratches shows a smooth build up of the force after which there are some small fluctuations. Despite the fluctuations seen in the forces the scratching process is relatively smooth and no evidence of large stick–slip events were seen to take place.

During the nanoscratching simulations, the material displaced as the indenter moves through the surface piles up along the edge of the scratch as shown in figures 16 and 17, for the rutile and anatase systems respectively. As with the indentation simulations, the greatest magnitude of pile-up is seen when scratching the rutile (001) surface, where material is densely packed along the sides of the scratch to a peak height of three atomic layers. On the other hand, the pile-up created during the scratch of the anatase {100} surface is extremely sparse, with a peak of only two layers of atoms. Analysis of the piled-up material shows that it is amorphous and is of a

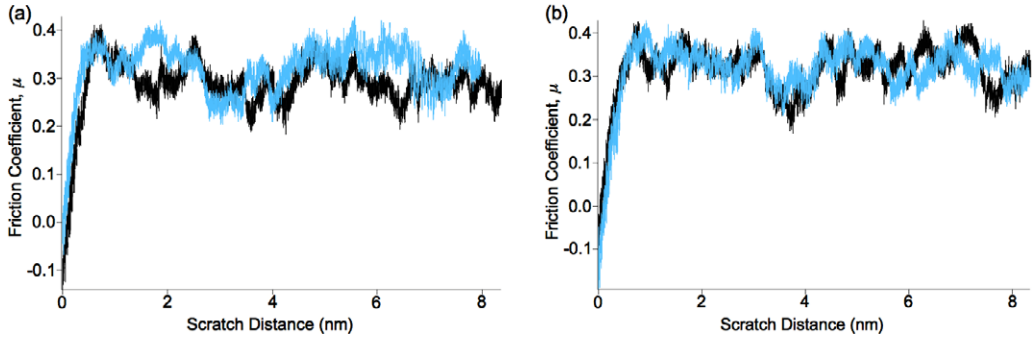

Figure 18. The friction between the indenter and surface during the scratches into the rutile (a) (001) (light) and {110} (1 × 1) reconstructed (dark) surfaces and the anatase (b) {100} (dark) and (001) (light) surfaces.

Table 3. The increase in density of a 4 nm × 4 nm × 2 nm region beneath the indenter compared to the number of atoms in the pile-up after the 18 Å indentations.

Surface	Density increase (%)	Number of piled-up atoms
Rutile (001)	2.0	906
Rutile {110}	3.3	404
Anatase {100}—A	4.6	194
Anatase {100}—B	4.9	181
Anatase (001)	3.0	431

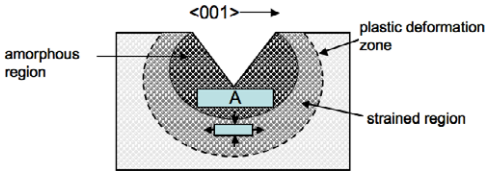

Figure 19. A diagram illustrating the plastic deformation zone after indenting anatase {100} to a depth of 18 Å. The arrows show the compression and expansion of the unit cell in the vertical and lateral directions. Region A represents the volume used to calculate the density in table 3.

similar amount for the rutile {110} and anatase (001) systems, with an average height of 4.5 Å.

The coefficient of friction is defined as

$$\mu = \frac{F_T}{F_N}, \tag{5}$$

where F_T is the tangential force and F_N is the normal force during the scratching simulation. Figure 18 shows the friction coefficients during the 6 Å scratches along the different TiO_2 surfaces. During the scratching stage of the simulation the normal force stays relatively stable, therefore, the overall shape of the friction coefficient curve is similar to that of the tangential force (figure 15). Of great interest is the fact that despite the tangential forces being considerably higher in the rutile scratches, the friction coefficient in both the rutile and anatase simulations are very similar, varying between 0.28 and 0.38.

During the indentation and scratching simulations, the anatase surfaces have produced a small amount of pile-up. In particular the anatase {100} surface shows very little material being deposited onto the surface of the lattice. In addition, an approximate count shows that the number of atoms displaced in the indentation site is greater than the number deposited on the surface. Therefore, there is significant densification beneath the surface. Table 3 shows that for orientations with relatively low numbers of piled-up atoms above the surface, there is a marked increase in density in the region beneath the indentation site.

Values given in table 3 are approximate, since to quantify density over a small volume is difficult due to finite size effects and the large difference in atomic weight between titanium and oxygen atoms. Figure 19 illustrates the deformation region in anatase {100} for the 18 Å indentation. The plastic deformation zone around the indent consists of an amorphous inner region surrounded by a region where the unit cells are strained but the atoms within the cells are still in the same relative positions. These cells are elongated in the ⟨001⟩ direction but compressed in the direction normal to the surface.

Table 4. The Q_4 parameter calculated for the titanium and oxygen atoms in the perfect TiO_2 phases.

TiO_2 polymorph	Q_4 parameter for titanium	Q_4 parameter for oxygen
Rutile	0.74	0.45
Anatase	0.65	0.69
Brookite	0.69	0.73

The nature of the densification in the anatase {100} indentation simulations leads to the question of whether the amorphous regions has any structure. One possible method to analyse this is by examining the change in coordination (number of nearest neighbours) of each atom. This analysis did not prove especially useful since only a small number of atoms changed coordination during indentation and the three main polymorphs of TiO_2, rutile, anatase and brookite share the same coordination numbers, as well as similar nearest neighbour distances. As a result the method of Steinhardt *et al* was used [30]. The Q_4 parameter defined in this method evaluates bond spherical harmonics to examine the local environment of an atom and can distinguish between different crystalline phases. The values in table 4 show the Q_4 parameter of atoms in the ideal lattice sites of the different TiO_2 polymorphs.

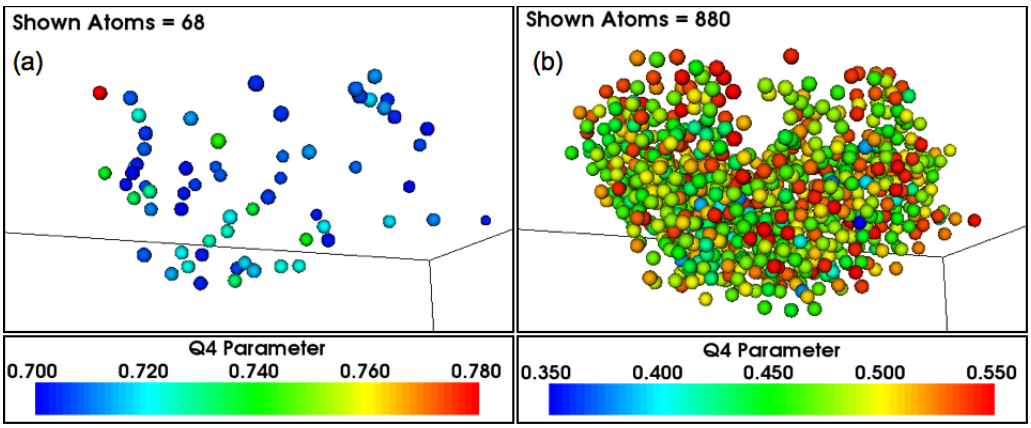

Figure 20. The Q_4 parameter of the titanium (a) and oxygen (b) atoms in the anatase {100} lattice after indenting to a depth of 18 Å. The filter range is set to show atoms with a Q_4 parameter which is close to the value of similar atoms in the rutile structure.

The Q_4 parameter after indenting the anatase {100} surface, with indenter orientation B, is shown in figure 20. A substantial number of oxygen atoms around the indentation site have a Q_4 parameter close to that of an oxygen atom in the rutile structure, however, the range of values is quite wide. On the other hand, there are virtually no titanium atoms which have had a shift in local environment from an anatase to rutile structure. If all possible values of the Q_4 parameter are viewed, there are a considerable number of titanium atoms which have had a decrease in Q_4 parameter around the indentation site (figure 21). This drop in the Q_4 parameter of titanium atoms is a feature seen in all of the anatase simulations, irrespective of crystal orientation.

Although large numbers of atoms around indentation and scratch sites have had changes in Q_4 parameter in rutile and anatase, there is no evidence of a phase change. There are no regions where both titanium and oxygen atoms have rearranged to obtain another known TiO_2 structure. However it may be possible to use the Q_4 parameter to define the extent of a plastic deformation zone around the indent, for example that volume in which the Q4 parameter has changed by a given amount such as the region shown in figure 20(b).

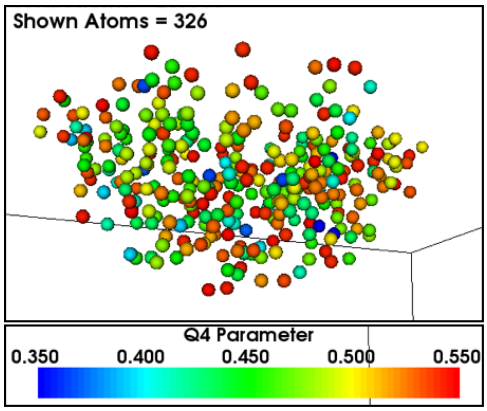

Figure 21. The Q_4 parameter of the titanium atoms in the anatase {100} lattice after an indentation simulation to 18 Å. The Q_4 parameter of these atoms is different to the three main polymorphs of TiO_2.

4. Conclusions

Pile-up patterns during both the indentation and scratching simulations into the TiO_2 lattices were found to be dependent on the surface structure with the (001) surface of the denser rutile polymorph having the greatest pile-up. Pile-up on the rutile {110} (1 × 1) reconstructed surface and the anatase (001) surface turned out to be quite similar after both indenting and scratching. The anatase {100} surface had much less pile-up during the indentation and scratching, with a densification of the material beneath the surface. There was no evidence of dislocation emission during indentation for either polymorph.

The friction coefficients, μ, found during the nanoscratch simulations of the different materials were all very similar although the forces required for both the indenting and scratching stages varied considerably for the different rutile and anatase surfaces. All four surfaces considered were found to have a coefficient of friction between 0.28 and 0.38.

The contact pressure and the Young's modulus of the TiO_2 polymorphs, were found to be in reasonable agreement with experiment, bearing in mind the limitations of the model. In anatase, the plastic deformation zone around the tip was found to consist of an amorphous region surrounded by a region where the unit cells remained compressed after tip extraction. Structural changes after indentation were identified using the Q4 parameter defined by Steinhardt *et al* [30] but no easily identifiable new phases could be found.

Acknowledgments

This work was funded by EPSRC (EP/C524322/1) with industrial support provided by Pilkington Group Ltd and Applied Multilayers Ltd. Thanks go to Loughborough University's high performance computing centre for providing facilities to run simulations. Useful discussions with Professor Steve Bull and Dr Jinju Chen were also much appreciated.

References

[1] Smith R, Christopher D, Kenny S, Richter A and Wolf B 2003 Defect generation and pile up of atoms during nanoindentation of Fe single crystals *Phys. Rev.* B **67** 245405

[2] Christopher D, Smith R and Richter A 2001 Nanoindentation of carbon materials *Nucl. Instrum. Methods Phys. Res.* B **180** 117–24

[3] Mulliah D, Kenny S D, Smith R and Sanz-Navarro C F 2004 Molecular dynamics simulations of nanoscratching of silver *Nanotechnology* **15** 243–9

[4] Smith R, Mulliah D, Kenny S D, McGee E, Richter A and Gruner M 2005 Stick slip and wear on metal surfaces *Wear* **259** 459–66

[5] Mulliah D, Kenny S D, McGee E, Smith R, Richter A and Wolf B 2006 Atomistic modelling of ploughing friction in silver, iron and silicon *Nanotechnology* **17** 1807–18

[6] Kenny S D, Mulliah D, Sanz-Navarro C F and Smith R 2005 Molecular dynamics simulations of nanoindentations and nanoscratching *Phil. Trans. R. Soc.* A **363** 1949–59

[7] Ho J and Farkas D 2007 Interaction of lattice dislocations with a grain boundary during nanoindentation simulation *Mater. Lett.* **61** 868–71

[8] Zimmermann J A, Kelchner C L, Klein P A, Hamilton J C and Foiles S M 2001 Surface step effects on nanoindentation *Phys. Rev. Lett.* **87** 5507

[9] Feichtinger D, Derlet P M and Van Swygenhoven H 2003 Atomistic simulations of spherical indentations in nanocrystalline gold *Phys. Rev.* B **67** 4113

[10] Ye Q, Liu P Y, Tang Z F and Zhai L 2007 Hydrophilic properties of nano-TiO_2 thin films deposited by rf magnetron sputtering *Vacuum* **81** 627–31

[11] Zywitzki O 2004 Structure and properties of crystalline titanium oxide layers deposited by reactive pulse magnetron sputtering *Surf. Coat. Technol.* **180/181** 538–43

[12] Wyckoff R W G 1963 *Crystal Structures* vol 1 (New York: Wiley)

[13] Diebold U 2003 The surface science of titanium dioxide *Surf. Sci. Rep.* **48** 53–229

[14] Liang Y, Gan S, Chambers S A and Altman E I 2001 Surface structure of anatase TiO_2(001): reconstruction, atomic steps, and domains *Phys. Rev.* B **63** 235402

[15] Gao W, Wang C M, Wang H Q, Henrich V E and Altman E I 2004 Growth and surface structure of vanadium oxide on anatase (001) *Surf. Sci.* **559** 201–13

[16] Brenner D W 1990 Emperical potential for hydrocarbons for use in simulating the chemical vapor deposition of diamond films *Phys. Rev.* B **42** 9458–71

[17] Brenner D W 1992 Emperical potential for hydrocarbons for use in simulating the chemical vapor deposition of diamond films *Phys. Rev.* B **46** 1948 (erratum)

[18] Biersack J, Ziegler J and Littmark U 1985 *The Stopping and Range of Ions in Solids* (Oxford: Pergamon)

[19] Matsui M and Akaogi M 1991 Molecular dynamics simulations of the structural and physical properties of the four polymorphs of TiO_2 *Mol. Simul.* **6** 239–44

[20] Rankin W T 2005 DPMTA—a distributed implementation of the parallel multipole *Tree Algorithm* Dept of Electrical Engineering, Duke University

[21] Berendsen H J C, Postma J P M, van Gunsteren W F, DiNola A and Haak J R 1984 Molecular dynamics with coupling to an external bath *J. Chem. Phys.* **81** 3684–90

[22] Smith R 2005 *Atomic Ion Collisions in Solids and at Surfaces* (Cambridge: Cambridge University Press)

[23] Haile J M 1992 *Molecular Dynamics Simulations* (New York: Wiley)

[24] Ashbee K H G and Smallman R E 1963 The plastic deformation of titanium dioxide single crystals *Proc. R. Soc.* A **274** 195–205

[25] Ashbee K H G, Smallman R E and Williamson G K 1963 Stacking faults and dislocations in titanium dioxide with special reference to non-stoichiometry *Proc. R. Soc.* A **276** 542–52

[26] Blanchin M G, Bursill L A and Lafage C 1990 Deformation and miscrostructure of rutile *Proc. R. Soc.* A **429** 175–202

[27] Oliver W C and Pharr G M 1992 An improved technique for determining hardness and elastic modulus using load and displacement sensing indentation experiments *J. Mater. Res.* **7** 1564–83

[28] McGee E, Smith R and Kenny S D 2007 Multiscale modelling of nanoindentation *Int. J. Mater. Res.* **98** 430–7

[29] Oliver W C, Pharr G M and Brotzen F R 1992 On the generality of the relationship among contact stiffness, contact area, on the generality of the relationship among contact stiffness, contact area, on the generality of the relationship among contact stiffness, contact area and elastic modulus during indentation *J. Mater. Res.* **7** 613–7

[30] Steinhardt P J, Nelson D R and Ronchetti M 1983 Bond-orientational order in liquids and glasses *Phys. Rev.* B **28** 784–805